**Smart Structures and Systems**, *Vol. 29, No. 5 (2022) 729-746*
https://doi.org/10.12989/sss.2022.29.5.729


# Nonlinear structural model updating based on the Deep Belief Network

Ye Mo [1], Zuo-Cai Wang*[1,2], Genda Chen [3], Ya-Jie Ding [1] and Bi Ge [1]

[1] *Department of Civil Engineering, Hefei University of Technology, Hefei, Anhui, 23009, China*
[2] *Anhui Engineering Research Center for Civil Engineering Disaster Prevention and Mitigation, Hefei, Anhui, 230009, China*
[3] *Department of Civil, Architectural, and Environmental Engineering, Missouri University of Science and Technology, Rolla, 65409, USA*

(*Received August 21, 2020, Revised May 19, 2021, Accepted March 15, 2022*)

**Abstract.** In this paper, a nonlinear structural model updating methodology based on the Deep Belief Network (DBN) is proposed. Firstly, the instantaneous parameters of the vibration responses are obtained by the discrete analytical mode decomposition (DAMD) method and the Hilbert transform (HT). The instantaneous parameters are regarded as the independent variables, and the nonlinear model parameters are considered as the dependent variables. Then the DBN is utilized for approximating the nonlinear mapping relationship between them. At last, the instantaneous parameters of the measured vibration responses are fed into the well-trained DBN. Owing to the strong learning and generalization abilities of the DBN, the updated nonlinear model parameters can be directly estimated. Two nonlinear shear-type structure models under two types of excitation and various noise levels are adopted as numerical simulations to validate the effectiveness of the proposed approach. The nonlinear properties of the structure model are simulated via the hysteretic parameters of a Bouc-Wen model and a Giuffré-Menegotto-Pinto model, respectively. Besides, the proposed approach is verified by a three-story shear-type frame with a piezoelectric friction damper (PFD). Simulated and experimental results suggest that the nonlinear model updating approach has high computational efficiency and precision.

**Keywords:** DBN; instantaneous parameters; nonlinear model updating; vibration responses

## 1. Introduction

In the last several decades, the finite element model updating (FEMU) technologies have made significant progress (Brownjohn *et al.* 2003, El-Borgi *et al.* 2005, Mordini *et al.* 2007, Weng *et al.* 2011, Lei *et al.* 2012, Zhang *et al.* 2013, Altunisik and Bayraktar 2017, Asadollahi *et al.* 2018, Hofmeister *et al.* 2019, Hoa *et al.* 2020). However, when structures are inevitably subjected to the natural environment or extreme loads during the service term, they usually show apparent nonlinearity and complex nonlinear dynamic behavior. In these cases, it is challenging to get accurate revised results using the model updating method based on the structural linear assumption theory. Therefore, it is essential to exploit a high-precision nonlinear FEMU strategy. The research on the nonlinear model updating of structures under extreme loads has not only theoretical significance but also realistic engineering value for structural damage diagnosis, health monitoring, and other fields. Moreover, it is an essential direction for developing the architectural model updating theory.

The nonlinear model can be rectified by the nonlinear structure parameters, and the nonlinearity of the nonlinear structure can be simulated by defining hysteresis models. Thus, the nonlinear FEMU can be attributed to identifying the hysteretic parameters. Some scholars applied the time-domain method to update the nonlinear model. Such as Astroza *et al.* (2016) proposed a FE model updating method combining simulated annealing (SA) with the unscented Kalman filter (UKF). Naranjo *et al.* (2020) proposed a novel hybrid unscented Kalman Filter-Harmony Search algorithm and successfully updated the FE model of a benchmark footbridge. The other methods calibrate nonlinear models according to the nonlinear characteristics of measured vibration responses. For example, Hemez *et al.* (2001) proposed the concept of the relationship between nonlinear models and test data and introduced the concept of nonlinear model updating. Yuen *et al.* (2011) proposed a Bayesian method for updating dynamic methods by using response time-history and modal measurements of a dynamical system. Naseralavi *et al.* (2016) developed a novel FEMU method to minimize the difference between the acceleration of the actual damaged structure and that of the simulated one. Ni and Ye (2019) presented a decentralized method for identifying the nonlinear parameters based on the dynamic responses of the subset. The time-frequency domain method to update the nonlinear model has attracted widespread attention in recent years. Asgarieh *et al.* (2014) developed a nonlinear FEMU method by applying the identified time-varying modal parameters. Their method employed the identified instantaneous frequency and mode shape as the optimization target to calibrate the hysteretic material parameters. Wang *et al.* (2015) presented a strategy for nonlinear FEMU by applying the instantaneous characteristics of the decomposed vibration responses.

Generally, the nonlinear FEMU can be summed up as

*Corresponding author, Professor,
E-mail: wangzuocai@hfut.edu.cn



ISSN: 1738-1584 (Print), 1738-1991 (Online)

the solution to an optimization problem. There will often be difficulties in the optimization process, such as quickly falling into local optimums, low optimization efficiency, and promptly being affected by measurement errors. Artificial neural networks (ANNs), due to their strong learning generalization ability and noise immunity, have been widely used in FEMU technologies. Yun and Bahng (2000) used the BP neural network to identify the stiffness parameters of complex structural systems. Chih-Chieh and Chin-Hsiung (2001) proposed a modeling and identification method of the discrete nonlinear hysteretic system based on the multilayer neural network. Lu and Tu (2004) proposed a two-level ANN-based FEMU method to identify structural parameters and damping ratios. Zapico *et al.* (2008) update the FEM of a small steel frame by the multilayer perceptron. Hasancebi and Dumlupinar (2013) proposed a novel ANN-based method to update the linear and nonlinear FEMs of an RC bridge. Park *et al.* (2017) used the ANN to express the relationship between the bridge responses and the rotating spring constants and proposed a FEMU method considering the boundary conditions. More recently, various latest ANN techniques have been widely used in civil engineering. Li *et al.* (2019) applied the Fully Convolutional Network (FCN) to detect multiple damages of concrete structures at pixel level and successfully detect four damage states of concrete. Zhou *et al.* (2020) used machine vision technology and deep learning algorithms to determine the spatial and temporal load distribution of vehicle loads on long-span Bridges. Their method can effectively predict the weight, type, position, and other information of vehicles. Huang *et al.* (2021) proposed a new compressive sensing method to identify cracks on the surface of structures, which can solve various practical problems of automatic crack segmentation.

The Deep Belief Network (DBN) is a deep learning model proposed by Hinton and Salakhutdinov (2006). Le Roux and Bengio (2010) pointed out that compared to shallow ANNs, the DBN can get the desired modeling accuracy with fewer hidden neurons. The DBN learning process consists of unsupervised learning and supervised learning. The unsupervised learning process is used to initialize the weights of the DBN, which is better than the random initialization of weights in other ANNs. The supervised learning uses the error back-propagation algorithm to fine-tune the initial weights generated by unsupervised learning. Because DBN has the practical ability to extract features from sample data, it is widely used in nonlinear system modeling (Qiao *et al.* 2018, Xu *et al.* 2019).

Due to the strong nonlinear mapping ability and anti-noise ability of the DBN, a DBN-based nonlinear structural model updating method is proposed. The uniform design method generates a certain number of nonlinear model parameters. In addition, the corresponding instantaneous parameters of the decomposed mono-component vibration responses are obtained by the discrete analytical mode decomposition (DAMD) method and the Hilbert transform (HT) (Wang *et al.* 2017). Then, the DBN model is trained by the training set that contains the extracted instantaneous parameters as input and the nonlinear model parameters as output. Finally, the updated nonlinear model parameters are exported directly by feeding the instantaneous parameters of the measured vibration responses into the well-trained DBN. A Bouc-Wen model and a Giuffré-Menegotto-Pinto model are numerically investigated to testify the effectiveness and applicability of the presented methodology. Besides, a three-story building model with a piezoelectric friction damper (PFD) is an experimental example.

## 2. Theoretical background

### 2.1 Instantaneous parameters extraction

The DAMD method is a time-frequency analysis method proposed by Wang *et al.* (2017), which can effectively separate the signals with time-varying closely spaced frequency components into multiple mono-component signals.

Assuming that $x(t)$ consists of a series of mono-component signals $x_i(t)$ ($i$=1, 2, ..., $n$), $x(t)=\sum_{i=1}^{n} x_i(t)$. The frequency corresponding to the mono-component signal $x_i(t)$ is $\omega_1(t)$, $\omega_2(t)$, …, $\omega_n(t)$. The $i$-th mono-component $x_i^{(d)}(t)$ can be expressed as

$$x_i^{(d)}(t) = s_i(t) - s_{i-1}(t) \quad (i = 2,3,\ldots,n) \tag{1}$$

where $x_1^{(d)}(t)=s_1(t)$ and $s_i(t)$ are written as

$$s_i(t) = \sin\left[\int_{-\infty}^{t} \omega_{bi}(\tau)d\tau\right] H\{x(t)\cos\left[\int_{-\infty}^{t} \omega_{bi}(\tau)d\tau\right]\} - \cos\left[\int_{-\infty}^{t} \omega_{bi}(\tau)d\tau\right] H\{x(t)\sin[\int_{-\infty}^{t} \omega_{bi}(\tau)d\tau]\} \quad (i=1,2,\ldots,n-1) \tag{2}$$

where $H(\cdot)$ denotes the HT operation, and $\omega_{bi}$ represents the time-varying cutoff frequency.

For a nonlinear MDOF system, the equation of motion is written as (Feldman 1997)

$$\boldsymbol{M}(t)\ddot{\boldsymbol{x}}(t) + \mathbf{C}(t)\dot{\boldsymbol{x}}(t) + \boldsymbol{K}(t)\boldsymbol{x}(t) = \boldsymbol{f}(t) \tag{3}$$

In Eq. (3), $\boldsymbol{M}(t)$, $\boldsymbol{C}(t)$, $\boldsymbol{K}(t)$ represent the mass, damping, and stiffness matrices that vary with time.

The structural vibration responses expressed in Eq. (3) are usually composed of multiple mono-components $x_l^i(t)$ composed of the frequency and amplitude varying with time (Wang *et at.* 2013). The $l$-th degree $x_l(t)$ of measured vibration responses are written as

$$x_l(t) = \sum_{i=1}^{n} x_l^{(i)}(t) \tag{4}$$

The analytical signal $Z_l^{(i)}$ of the $i$-th decomposed responses $x_l^i(t)$ is formulated as

$$Z_l^{(i)} = x_l^{(i)}(t) + H[x_l^i(t)] \tag{5}$$

The instantaneous amplitude and the instantaneous phase are written as

$$A(t) = \left|Z_l^{(i)}\right| = \sqrt{(x_l^{(i)}(t))^2 + (H[x_l^i(t)])^2} \tag{6}$$

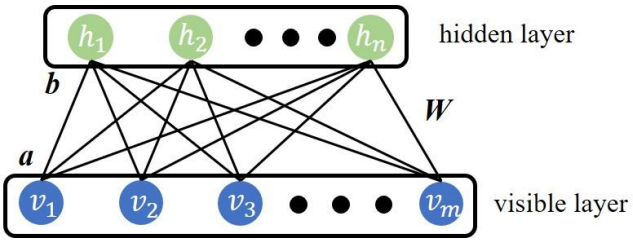


Fig. 1 The RBM model

$$\omega(t) = \arctg\frac{H[x_l^i(t)]}{x_l^{(t)}(t)} \tag{7}$$

The instantaneous frequency $f(t)$ is the first-order derivative of $\omega(t)$ concerning time, that is, $f(t)=\frac{d\omega(t)}{dt}$. The slow-varying part of the $f(t)$ can be obtained by the DAMD method, defined as $f_{sl}(t)$. In this paper, $A(t)$ and $f_{sl}(t)$ of the first-order mono-component are regarded as the instantaneous parameters.

### 2.2 DBN

The DBN model is a probabilistic generative model. It is formed by stacking multiple Restricted Boltzmann Machines (RBMs) (Hinton and Salakhutdinov 2006). At the bottom of the DBN model, the RBMs are trained to extract the features of sample data. Its top layer uses the supervised backpropagation (BP) neural network to fit the expected results. Consequently, the DBN can fit the complicated nonlinear functional relationships by directly mapping data from the input to output data. The structure and principles of RBM and the DBN will be further introduced in section 2.2.1 and section 2.2.2.

#### 2.2.1 RBM

Hinton and Sejnowski developed the RBM model, a generalized stochastic neural network. Statistics show that converting all probability distributions to energy models is reasonable. The RBM provides a learning model for training samples whose internal distribution is unknown (Pirmoradi *et al.* 2020) and has two layers of neurons. One layer of the RBM, called the visible layer, is composed of visible units, and the other is named the hidden layer, which is made up of hidden units. The connection between neurons is no connection within the layer but a full connection between the layers (Hinton 2012). Fig. 1 illustrates the RBM model.

Assumed that $\boldsymbol{v}=\{v_1,v_2,\ldots,v_{n_v}\}$ denotes the visible layer unit vector, $\boldsymbol{h}=\{h_1,h_2,\ldots,h_{n_h}\}$ denotes the hidden layer unit vector; $w$ represents the weight matrix; $\boldsymbol{a}$ is the bias vector of the visible layer, and $\boldsymbol{b}$ denotes the bias vector of the hidden layer. Since the RBM is an energy-based model, the energy function $E_\theta(\boldsymbol{v}, \boldsymbol{h})$ of all visible and hidden units can be described as

$$E_\theta(\boldsymbol{v},\boldsymbol{h}) = \sum_i^{n_v} a_i v_i - \sum_j^{n_h} b_j h_j - \sum_i^{n_v}\sum_j^{n_h} v_j w_{ij} h_j \tag{8}$$

In which $n_v$ denotes the number of visible units, and $n_h$ represents that of hidden units. Based on Eq. (8), the joint probability distribution of state $(\boldsymbol{v}, \boldsymbol{h})$ is written as

$$P_\theta(\boldsymbol{v},\boldsymbol{h}) = \frac{e^{-E_\theta(\boldsymbol{v},\boldsymbol{h})}}{Z_\theta} \tag{9}$$

where $Z_\theta=\sum_{\boldsymbol{v}}\sum_{\boldsymbol{h}} e^{-E_\theta(\boldsymbol{v},\boldsymbol{h})}$ is a normalized constant or named as the partition function (Mohamed *et al.* 2012). The probability distribution of the observation data, that is, the marginal distribution of $P_\theta$ can be formulated as

$$P_\theta(\boldsymbol{v}) = \sum_{\boldsymbol{h}} P_\theta(\boldsymbol{v},\boldsymbol{h}) = \frac{\sum_{\boldsymbol{h}} e^{-E_\theta(\boldsymbol{v},\boldsymbol{h})}}{Z_\theta} \tag{10}$$

Due to the special structure of the RBM, when the visible layer vector $\boldsymbol{v}$ is known, the conditional probability of the $j$-th hidden unit is formulated:

$$P_\theta(h_j = 1 | \boldsymbol{v}) = sigmoid(b_j + \sum_{i=1}^{m} w_{ji} v_i) \tag{11}$$

Similarly, the conditional probability of the $i$-th visible unit can be described as:

$$P_\theta(v_i = 1 | \boldsymbol{h}) = sigmoid(a_i + \sum_{j=1}^{n} w_{ji} h_j) \tag{12}$$

where $sigmoid(x)$ is named as the activation function.

The essence of the RBM model is to maximize the probability of coincidence between the trained RBM model and the input sample distribution through the training of sample data. Training the RBM is an unsupervised learning procedure. The output of the previous layer is regarded as the following layer input, and the energy of the RBM is minimized to initialize the weight of DBN. The weight matrix $\boldsymbol{w}$, the bias vector of the visible layer $\boldsymbol{a}$, and the bias vector $\boldsymbol{b}$ of the hidden layer can be obtained by maximizing the logarithm function on the samples as follow.

$$\begin{aligned}\{a_i, b_j, w_{ij}\} &= \arg\max F\,(a_i, b_j, w_{ij}) \\ &= \arg\max \sum_{l=1}^{L} LnP < v^l | (a_i, b_j, w_{ij}) >\end{aligned} \tag{13}$$

where $L$ is the number of training data.

As it is challenging to solve the above optimization problem, a contrastive divergence (CD) fast learning algorithm is used in this paper. This algorithm has become the standard algorithm for training the RBM. The k-step CD algorithm is summarized in Fischer and Igel (2014).

#### 2.2.2 DBN structure and training

As mentioned in section 2.2.1, the DBN is constructed by superposing multiple RBMs. The data is entered layer by layer. The classical DBN structure comprises multilayer RBMs and a monolayer BP network. The number of neurons is adjusted according to actual needs.

The training procedure of the DBN is mainly divided into two steps: unsupervised pre-training and supervised fine-tuning (Hinton *et al.* 2006). First, each layer of the RBM is trained independently and unsupervised to keep the characteristics of training data. Then the error between the

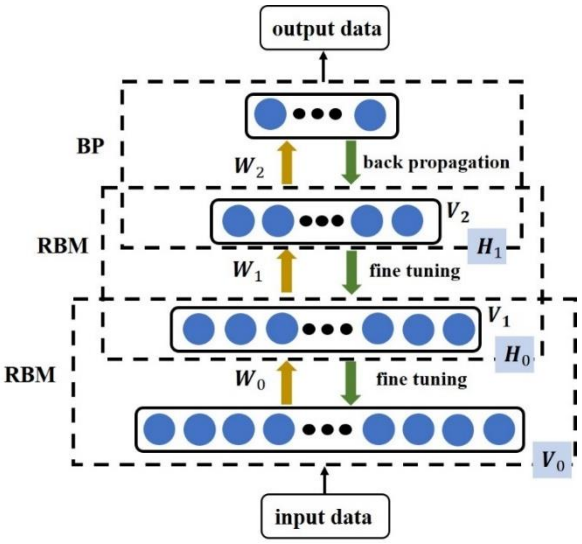


Fig. 2 The training process of the DBN

output and the predicted output is calculated, and the BP network is used to optimize further the initial weights set before. The BP network at the top layer of the DBN only needs to perform a partial search on the parameter space of the weight. It overcomes the shortcomings brought by the BP network randomly initialized weight parameters, such as easy to fall into local optimal and long training time. Fig. 2 demonstrates the training process of the DBN.

### *2.3 Nonlinear model updating based on the DBN*

For nonlinear FEMU, it is usually difficult to establish the relationship between the vibration response characteristics and nonlinear model parameters. As concluded from section 2.2, the DBN has a strong generalization ability and is suitable for obtaining complicated nonlinear function relationships. The information about nonlinear function relationships is stored in the input, weights, biases, and output of the DBN. Moreover, the weights and biases are obtained by training.

In the proposed method, the input is the instantaneous parameters of vibration responses, including the instantaneous amplitude $A(t)$ and the slow-varying parts of the instantaneous frequency $f_{sl}(t)$. The nonlinear model parameters are employed as the output. This paper adopts the DBN with three-layer RBM, and the number of neurons is determined by numerical experiments. Mathematically, the DBN is utilized to express the complicated nonlinear mapping accurately between input $\boldsymbol{X}$ and output $\boldsymbol{Y}$ as follows

$$\boldsymbol{Y} = g(\boldsymbol{A}, \boldsymbol{B}, \boldsymbol{W}, \boldsymbol{X}) \tag{14}$$

where the bias vector $\boldsymbol{A}$ of the visible units is composed of bias coefficients $a_i$; the bias vector $\boldsymbol{B}$ of the hidden units is formed of bias coefficients $b_j$, and the weight matrix $\boldsymbol{W}$ is composed of weight coefficients $w_{ij}^k$, which are expressed as

$$\boldsymbol{A} = \{a_1, a_2, a_3, \ldots, a_{n_v}\} \tag{15}$$

$$\boldsymbol{B} = \{b_1, b_2, b_3, \ldots, b_{n_h}\} \tag{16}$$

$$\boldsymbol{W} = \{w_{ij}^k,\ i = 1,\ldots,n_v;\ j = 1,\ldots,n_h;\ k = 1,2,3\} \tag{17}$$

The DBN-based nonlinear structural model updating strategy presented in this paper includes the following two steps:

(1) The DBN is initially trained with the original training samples.

(2) The performance of the initial training is evaluated by comparing the instantaneous parameters of the updated nonlinear model and that of measured vibration responses. If the discrepancy between them is large, the DBN will be retrained.

The objective of the initial training is to construct a direct nonlinear mapping relation between the extracted instantaneous parameters and the nonlinear model parameters, as shown in Fig. 3. The training samples are assumed nonlinear model parameters and the corresponding instantaneous parameters. Specifically, the uniform design method is applied to generate the nonlinear model parameter samples, making each sample point sufficiently representative. Then the corresponding instantaneous parameters are obtained by the DAMD method and the HT. Finally, the DBN is trained by the training samples. To speed up the convergence rate of the training process, standardized preprocessing of sample data is required, where the normalized function is

$$x^* = 2 \times \frac{x - x_{\min}}{x_{\max} - x_{\min}} - 1 \tag{18}$$

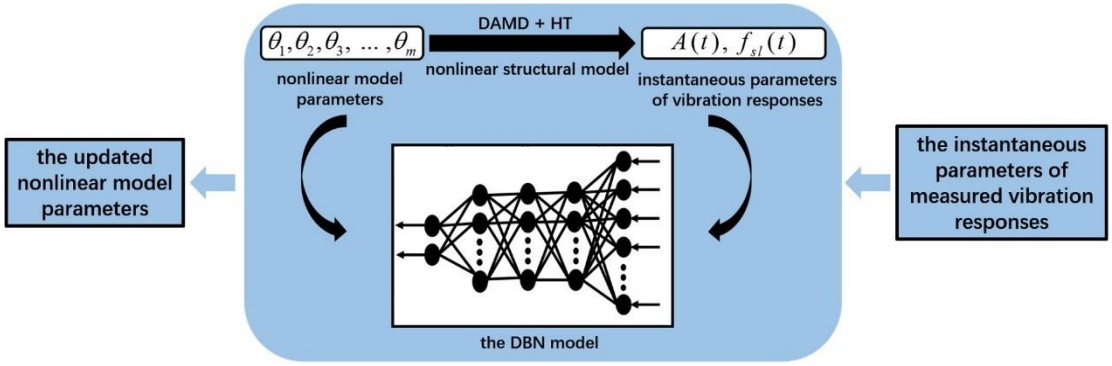


Fig. 3 The initial training of the DBN

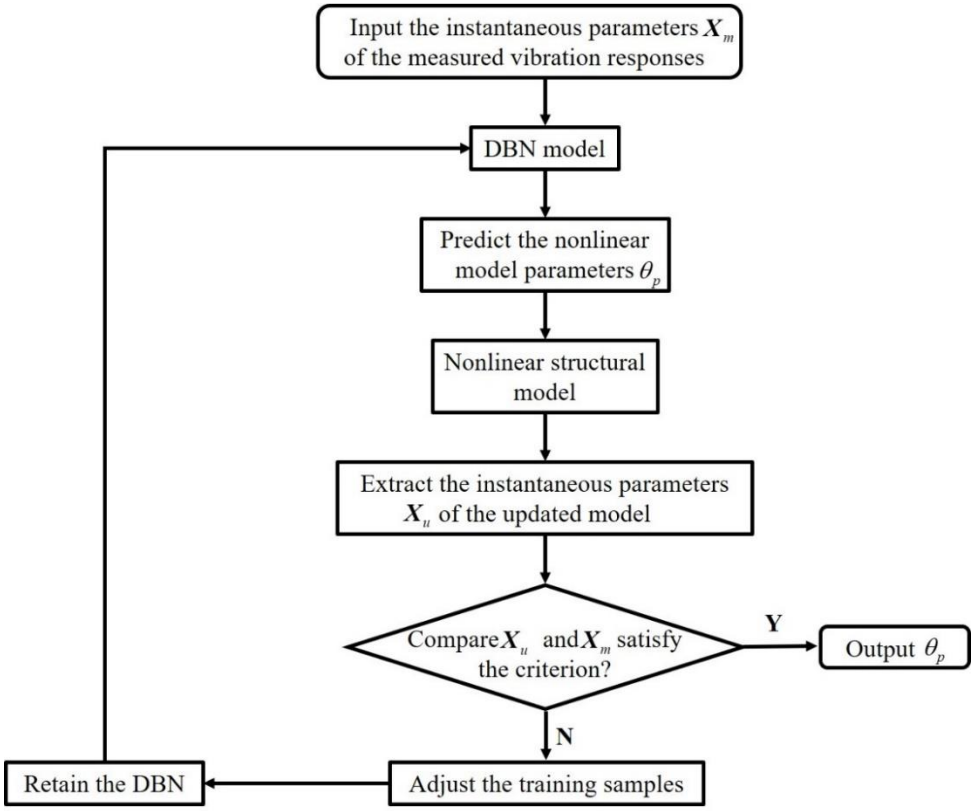


Fig. 4 The flow chart of the retraining process

After the initial training, it is crucial to evaluate the training performance. Based on a given criterion, the updated instantaneous parameters $\boldsymbol{X}_u$ are compared with the measured data $\boldsymbol{X}_m$. If the criterion cannot be satisfied, the DBN will be retrained. The retraining process will be repeated until the given criterion is met, as summarized in Fig. 4. The criterion may not be set too small or big. If it is set too large, it may cause the DBN to fail to characterize the relationship between input and output accurately. Besides, in actual engineering, the nonlinear structure model usually simplifies the actual structure to a certain extent, which leads to a specific difference between the calculated results of the nonlinear FEM and the measured values. Therefore, the criterion assumed in this paper is $\|\boldsymbol{X}_u\text{-}\boldsymbol{X}_m\|_2/\|\boldsymbol{X}_m\|_2 \leq 20\%$.

A dynamic adjustment method for generating samples is adopted in the retraining process, referred to Chang *et al.* (2000). When a new sample is added to the original samples, one of the initial samples is deleted. As a result, the total number of samples will not be changed. The new sample comprises the nonlinear model parameters updated based on the DBN and the corresponding instantaneous parameters. The sample deleted is the one with the largest relative error $E_{max}$, which is defined as follow

$$E_{max} = \max\left(\frac{\left\|\boldsymbol{X}^{\text{measured}} - \boldsymbol{X}^{i}\right\|_2}{\left\|\boldsymbol{X}^{\text{measured}}\right\|_2} \times 100\%,\ i = 1, 2, \ \ldots, n\right) \quad (19)$$

where $\boldsymbol{X}^{\text{measured}}$ denotes the instantaneous parameters of the measured vibration responses, $\boldsymbol{X}^i$ denotes the instantaneous parameters of the $i$-th sample.

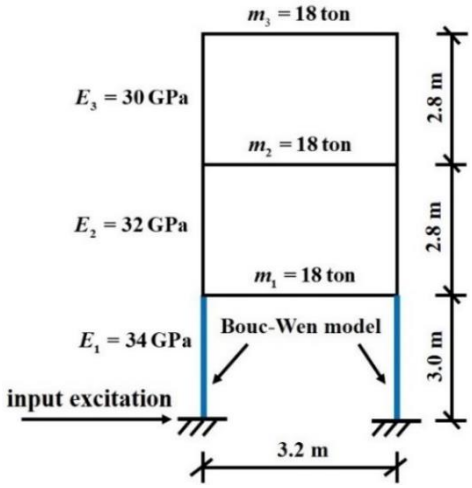


Fig. 5 The three-story nonlinear Bouc-Wen shear model

By replacing the sample with the largest relative error, the density of samples around the instantaneous parameters of the measured vibration responses can be increased.

## 3. Numerical verification

### *3.1 Nonlinear model updating for Bouc-Wen model*

#### *3.1.1 Instantaneous parameters extraction*

In this section, a three-story nonlinear structure model is adopted as the research object, as shown in Fig. 5. The linear parameters of the model are demonstrated in Fig. 5.

Table 1 The initial values of the hysteresis parameters of the Bouc-Wen model

| | $\alpha$ | $\beta$ | $\gamma$ | $\delta_v$ | $\delta_\eta$ | $n$ |
|---|---|---|---|---|---|---|
| initial values | 0.30 | 260 | 260 | 1.5 | 0.15 | 1.0 |

The columns of the 1st floor are set as nonlinear elements and other columns and beams as linear-elastic elements. The Bouc–Wen model with six nonlinear parameters to be updated is used as the simulated nonlinear hysteresis model. These parameters are $\alpha$, $\beta$, $\gamma$, $\delta_v$, $\delta_\eta$, and $n$, respectively. Where $\alpha$ is the ratio of linear to nonlinear stiffness; $\beta$, $\gamma$ are the basic control parameters of hysteresis loop shape; $n$ is the sharpness parameter of yield; $\delta_v$ is the strength degradation factor, and $\delta_\eta$ is stiffness degradation factor. Table 1 lists the initial values of the nonlinear parameters. The nonlinear model is assumed to be subjected to the Northridge earthquake, whose acceleration record is illustrated in Fig. 6. Assumed that the simulated acceleration on the 3rd floor is the measured response, as demonstrated in Fig. 7. The sampling frequency is set as 240 Hz. The Fourier spectrum of the acceleration and the nonlinear force-displacement hysteretic curve is presented in Figs. 8 and 9, respectively. Fig. 9 demonstrates that the model exhibits obvious nonlinearity under seismic excitation. The instantaneous amplitude $A(t)$ and slow-varying part of the instantaneous frequency $f_{sl}(t)$ of the acceleration are obtained by the DAMD method and the HT. Figs. 10 (a)-(b) show the instantaneous characteristics

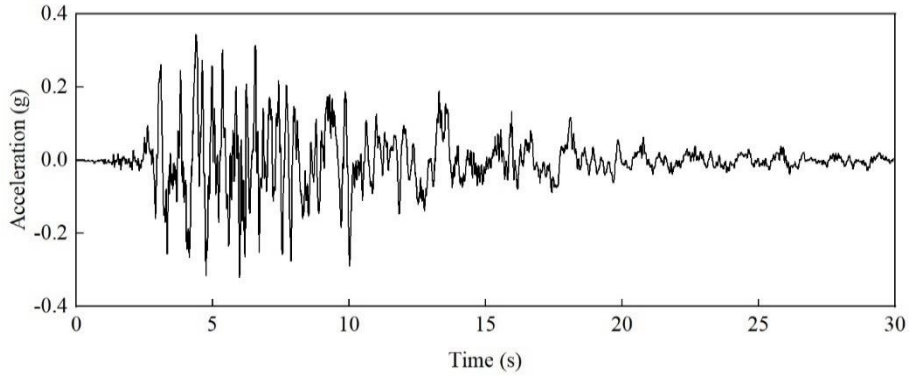


Fig. 6 The acceleration record of the Northridge earthquake

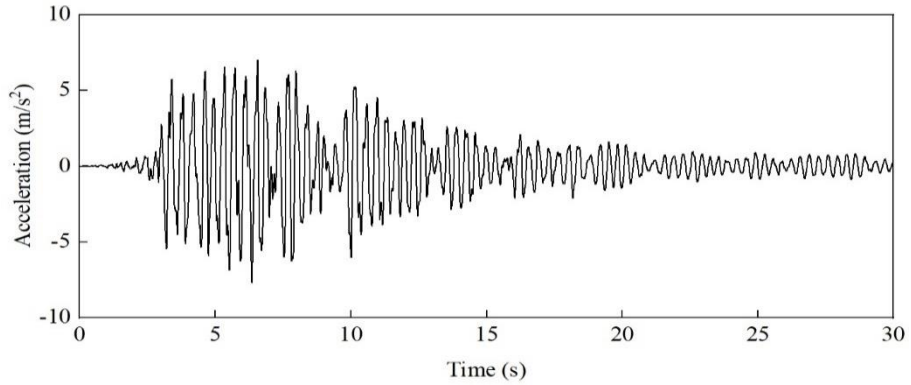


Fig. 7 The acceleration on the 3rd floor of the Bouc-Wen model

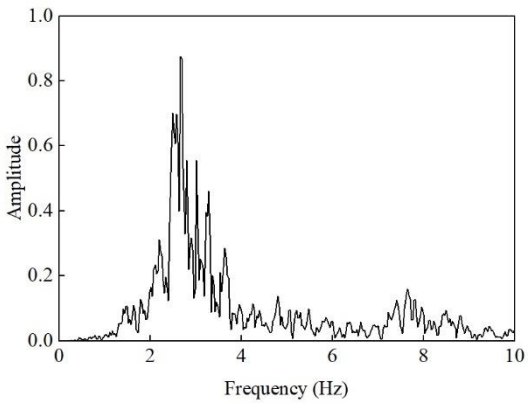


Fig. 8 The Fourier spectrum of the acceleration on the 3rd floor

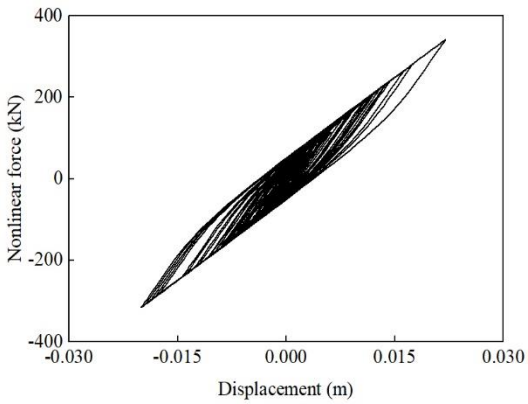


Fig. 9 The force-displacement hysteretic curve

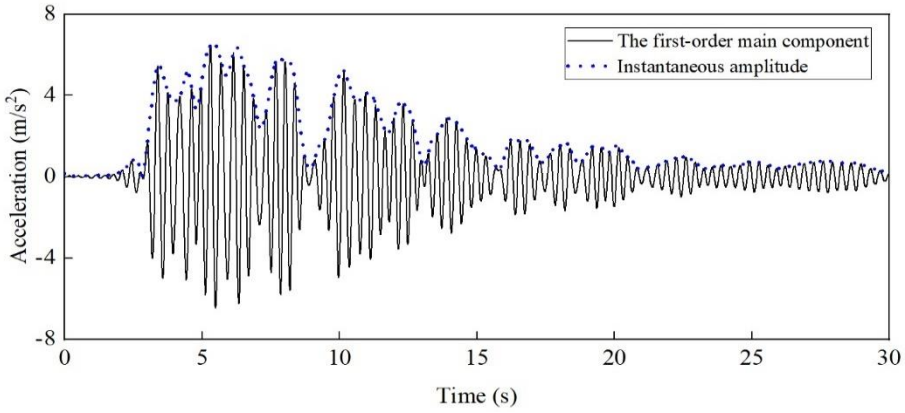


(a) The instantaneous amplitude

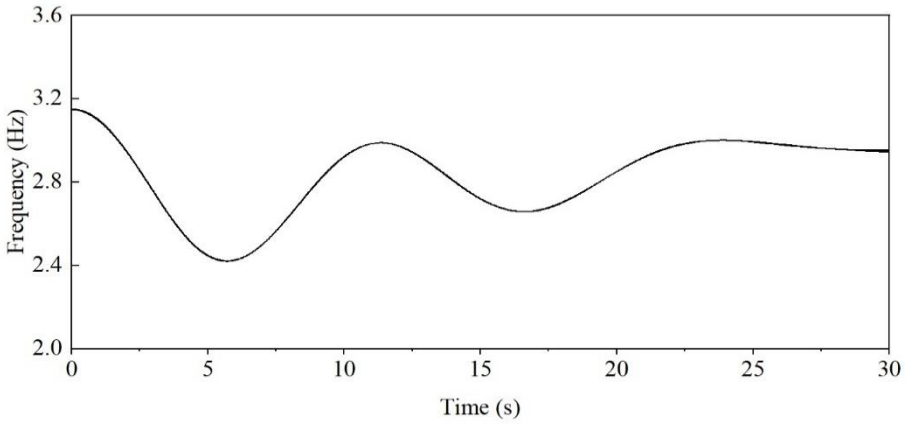


(b) The slow-varying part of the instantaneous frequency

Fig. 10 The instantaneous characteristics of the first main mono-component extracted from the Bouc-Wen model under seismic excitation

of the first-order main mono-component.

### *3.1.2 Nonlinear Bouc-Wen model updating under seismic excitation*

In the simulation, each parameter is uniformly divided into 60 levels within 25% fluctuation of the original, and 60 sets of nonlinear model parameters are generated by the uniform design matrix $U_{60}(60^6)$. The corresponding instantaneous parameters are extracted by the DAMD method and the HT. Then the DBN is trained by the generated training samples. The structure of the DBN will affect the updating results. Therefore, the numerical experimental method determines the DBN structure and learning parameters. By comparing the updating results obtained by different DBN models, the relevant parameters are finally determined: the number of neurons in the top BP network is 10, the learning rate is selected as 0.01, the learning times are 500, and the expected error is 0.0001.

Compared with the vibration responses, the extracted $A(t)$ and $f_{sl}(t)$ change slowly. Thus, it is unnecessary to apply all the measured data, which will save the computational cost of this method. However, the applied time series may simplify the preliminary distribution features if too few data points are selected. The impact of the number of selected data will be explored with four cases considered as follow,

Case 1: 100% of the instantaneous parameters are selected.

Case 2: 1% of the instantaneous parameters are selected with equal time intervals.

Case 3: 5% of the instantaneous parameters are selected with equal time intervals.

Case 4: 10% of the instantaneous parameters are selected with equal time intervals.

This paper utilizes two error indicators $E_f$ and $E_{acc}$ to evaluate the accuracy of the calibrated model, which are defined as (Wang *et al.* 2015)

$$E_f = \frac{\left\| f_{sl}^{measured}(t) - f_{sl}^{updated}(t) \right\|_2}{\left\| f_{sl}^{measured}(t) \right\|_2} \times 100\% \tag{20}$$

$$E_{acc} = \frac{\left\| A^{measured}(t) - A^{updated}(t) \right\|_2}{\left\| A^{measured}(t) \right\|_2} \times 100\% \tag{21}$$

Table 2 lists the optimal updated nonlinear model parameter and the error indicators under four cases. It shows that the DBN-based method rectifies the six hysteresis parameters with high efficiency and precision. Besides, when 10% of the data are selected, the revised results are better than those in Case 2 and 3. In this case, the two error indicators $E_f$ and $E_{acc}$ are 0.066% and 5.29%,

Table 2 The updated Bouc-Wen hysteresis parameters and the two error indicators under four cases

| | | $\alpha$ | $\beta$ | $\gamma$ | $\delta_v$ | $\delta_\eta$ | $n$ | $E_f$ (%) | $E_{acc}$ (%) |
|---|---|---|---|---|---|---|---|---|---|
| Exact values | | 0.300 | 260 | 260 | 1.5 | 0.15 | 1.0 | | |
| Updated values | Case1 | 0.285 | 239.2 | 245.8 | 1.32 | 0.15 | 1.01 | 0.065 | 5.22 |
| | Case2 | 0.294 | 243.4 | 241.1 | 1.34 | 0.15 | 1.01 | 2.85 | 4.88 |
| | Case3 | 0.285 | 242.6 | 238.8 | 1.36 | 0.15 | 1.02 | 0.095 | 5.65 |
| | Case4 | 0.280 | 236.5 | 247.7 | 1.43 | 0.15 | 1.00 | 0.066 | 5.29 |

respectively. It indicates that it is feasible for the proposed method to select 10% of the instantaneous parameters.

The acceleration comparison between the 3rd floor of the updated model and the exact structure is illustrated in Fig. 11. Figs. 12 (a)-(b) illustrate the comparison of the instantaneous characteristics of the first-order main mono-component. These results also verify the accuracy of the DBN-based method.

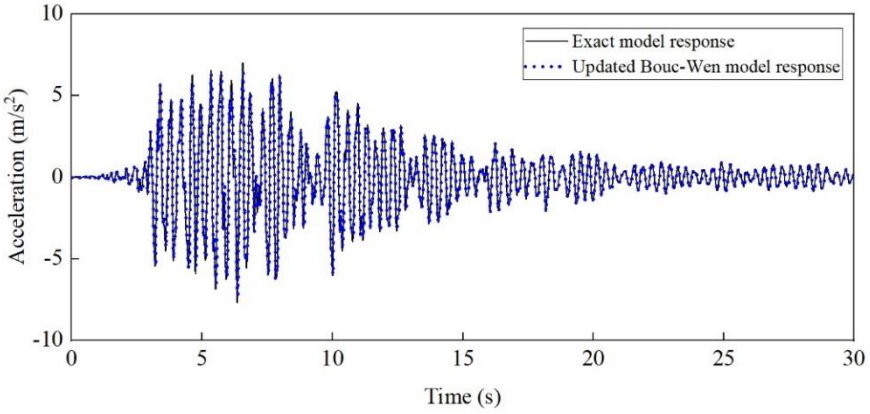


Fig. 11 The acceleration comparison between the updated Bouc-Wen model and the exact model

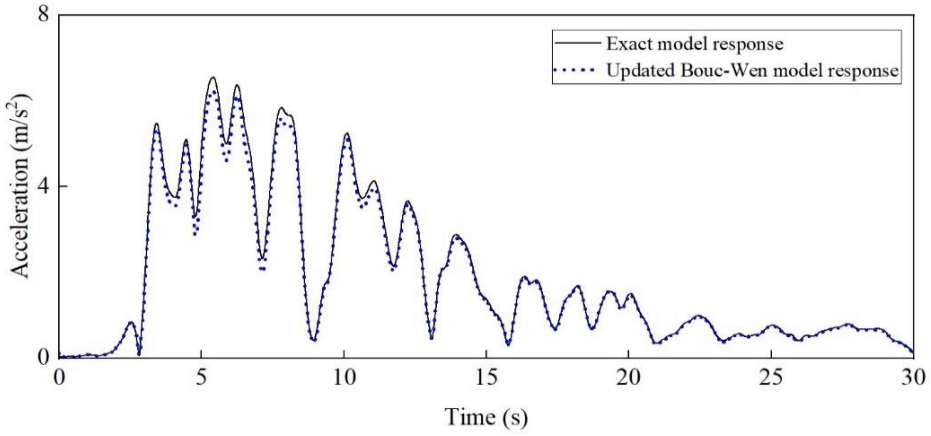


(a) The instantaneous amplitude

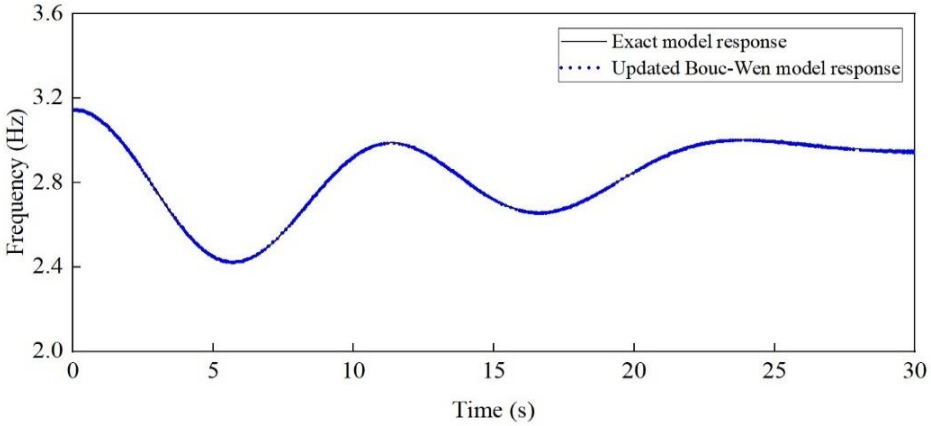


(b) The slow-varying portion of the instantaneous frequency

Fig. 12 The comparison of the instantaneous characteristics extracted from the first main mono-component between the updated Bouc-Wen model and the exact model

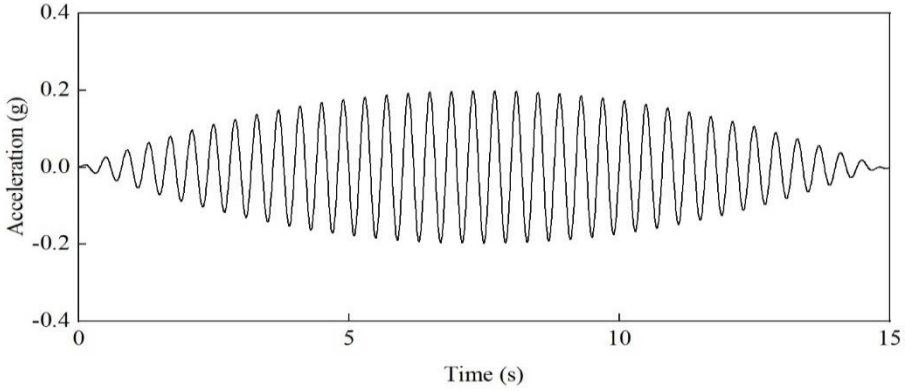


Fig. 13 The external harmonic excitation

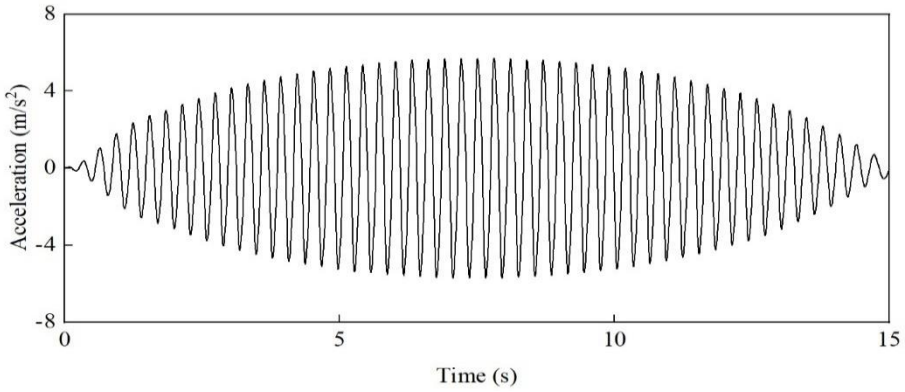


Fig. 14 The acceleration on the 3rd floor of the Bouc-Wen model under harmonic excitation

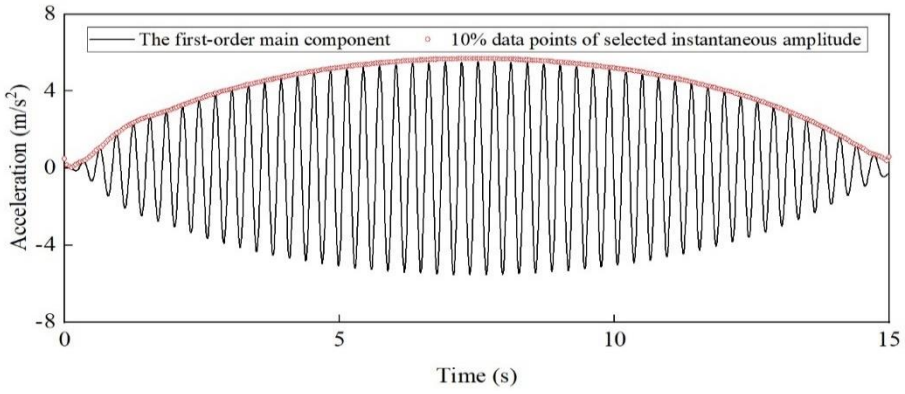


(a) The instantaneous amplitude

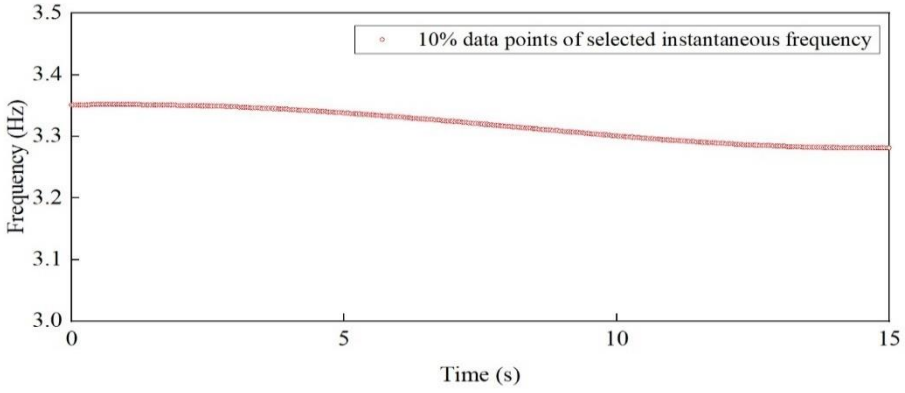


(b) The slow-varying part of the instantaneous frequency

Fig. 15 The instantaneous characteristics of the main mono-component extracted from the Bouc-Wen model under harmonic excitation

### 3.1.3 Nonlinear Bouc-Wen model updating under harmonic excitation

In section 3.1.2, the $f_{sl}(t)$ of the simulated acceleration subjected to earthquake excitation is successfully used to rectify the Bouc-Wen model. However, the nonlinear structure is often excited by harmonics or other narrowband excitations. In these circumstances, the $f_{sl}(t)$ is very close to the excitation frequency. As a result, it is necessary to investigate the validity of the presented method subjected to harmonic excitation.

The nonlinear model described in Section 3.1.1 is utilized as a simulated example. The external excitation is selected as $f_g=(-0.0036t^2+0.0544t)\times\sin(6.7\pi t)g$, where $g$ represents the gravitational acceleration. The loading duration is 15 seconds, and the sampling frequency is 240 Hz. The external harmonic excitation is illustrated in Fig. 13. To further verify the robustness of the method, the simulated acceleration are polluted with Gaussian white noise of 5%, 10%, 15%, and 20% noise-to-signal ratios (NSR). Where $P_{\text{noise}}=n\times P_{\text{signal}}$, $P_{\text{noise}}$ is the power of Gaussian white noise, $P_{\text{signal}}$ is that of the measured response signal without the influence of noise, and $n$ is the power ratio of noise and acceleration response signal. Fig. 14 demonstrates the simulated acceleration on the 3rd floor. According to the above numerical example, the uniformly selected 10% of instantaneous parameters can be used to update the Bouc-Wen model accurately. Therefore, in this section, 10% of data points are selected with equal time intervals as instantaneous parameters from the instantaneous amplitude and the slowly varying components of instantaneous frequency, respectively. The selected instantaneous parameters are shown in Figs. 15 (a)-(b).

Based on the uniform design method, 60 groups of nonlinear model parameters are obtained. Then, the corresponding instantaneous parameters are extracted. The instantaneous parameters are taken as the input, and the corresponding nonlinear model parameters as the output to train the DBN. The purpose of using DBN to update the nonlinear structural model is to minimize the difference between the vibration responses calculated by the calibrated model and the measured values. Therefore, the instantaneous parameters of the measured vibration response and the corresponding nonlinear model parameters are directly taken as the test samples. After calculation, the rectified hysteretic parameters and the two error indicators are illustrated in Table 3. It demonstrates that the error indicators increase gradually as the measurement NSR noise level increases. Specifically, $E_f$ and $E_{acc}$ with 20% NSR noise levels are 3.26% and 10.11%. These results verify the robustness of the presented method with noise effect.

Table 3 The rectified hysteretic parameters and the two error indicators of the Bouc-Wen model under harmonic excitation with different NSR noise level

| | | $\alpha$ | $\beta$ | $\gamma$ | $\delta_\nu$ | $\delta_\eta$ | $n$ | $E_f$ (%) | $E_{acc}$ (%) |
|---|---|---|---|---|---|---|---|---|---|
| Exact values | | 0.3 | 260 | 260 | 1.5 | 0.15 | 1.0 | | |
| Updated values | without noise | 0.273 | 248.7 | 240.9 | 1.40 | 0.15 | 1.00 | 0.073 | 2.53 |
| | with 5% noise | 0.255 | 278.7 | 257.0 | 1.26 | 0.15 | 1.00 | 0.094 | 4.47 |
| | with 10% noise | 0.269 | 248.8 | 225.7 | 1.50 | 0.15 | 1.06 | 0.087 | 7.08 |
| | with 15% noise | 0.266 | 251.3 | 236.2 | 1.32 | 0.15 | 1.06 | 3.23 | 7.51 |
| | with 20% noise | 0.283 | 239.2 | 226.0 | 1.31 | 0.15 | 1.05 | 3.26 | 10.11 |

The comparison between the 3rd floor acceleration response without noise/with the 5% noise effect of the calibrated nonlinear model and that of the actual model under harmonic excitation is shown in Fig. 16. Furthermore, the comparison of the $A(t)$ and $f_{sl}(t)$ are illustrated in Figs. 17(a)-(b). Such results also illustrate that the Bouc-Wen model can be calibrated with high efficiency under harmonic excitation.

To further prove the superiority of the proposed method in Bouc-Wen model correction, the correction accuracy and computational efficiency of the four nonlinear FEMU methods are compared. The four methods are based on the DBN, DAMD-DBN, DAMD-BP neural network, and DAMD-SA (Simulated Annealing global optimization algorithm). The results are shown in Fig. 18. The DBN-based updating algorithm directly uses the DBN to study the relationship between the acceleration response and the Bouc-Wen model parameters. The algorithm based on the VMD-BP refers to replacing the DBN with the BP neural network. The main steps of the algorithm are familiar with the proposed method. The specific content of the DAMD-SA algorithm can be referred to in the literature (Wang *et al.*

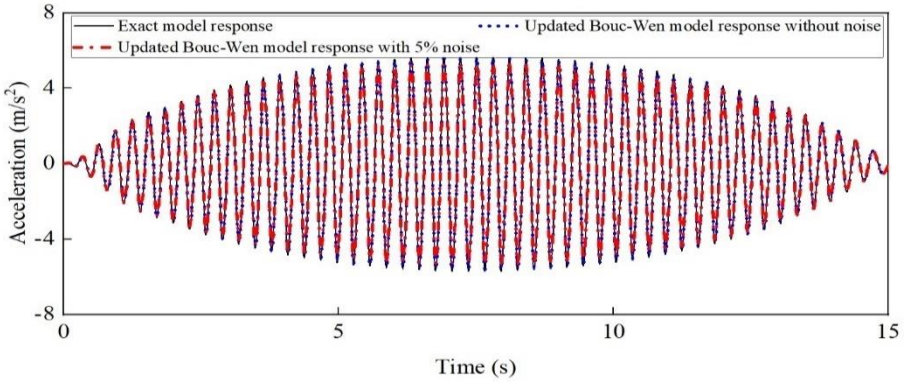


Fig. 16 The acceleration comparison between the updated Bouc-Wen model with 5% noise/without noise and the exact model under harmonic excitation

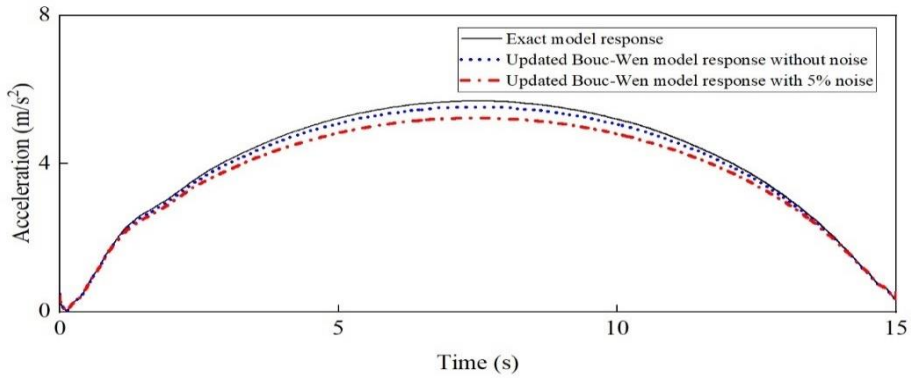


(a) The instantaneous amplitude

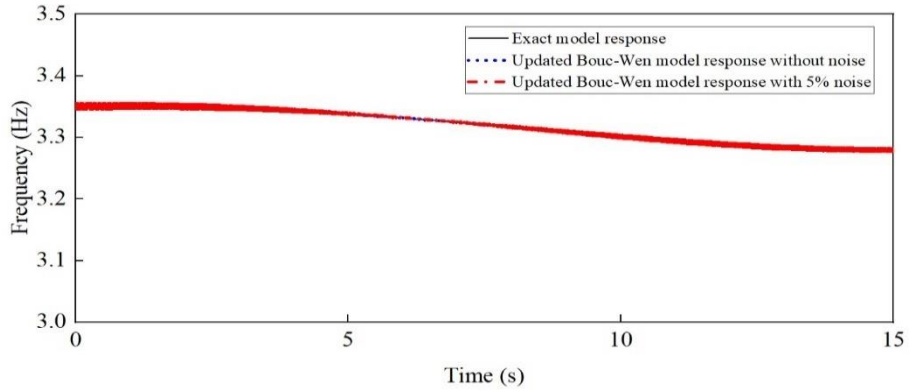


(b) The slow-varying portion of the instantaneous frequency

Fig. 17 The comparison of the instantaneous characteristics of the main mono-component between the updated Bouc-Wen model with 5% noise/without noise and the exact model under harmonic excitation

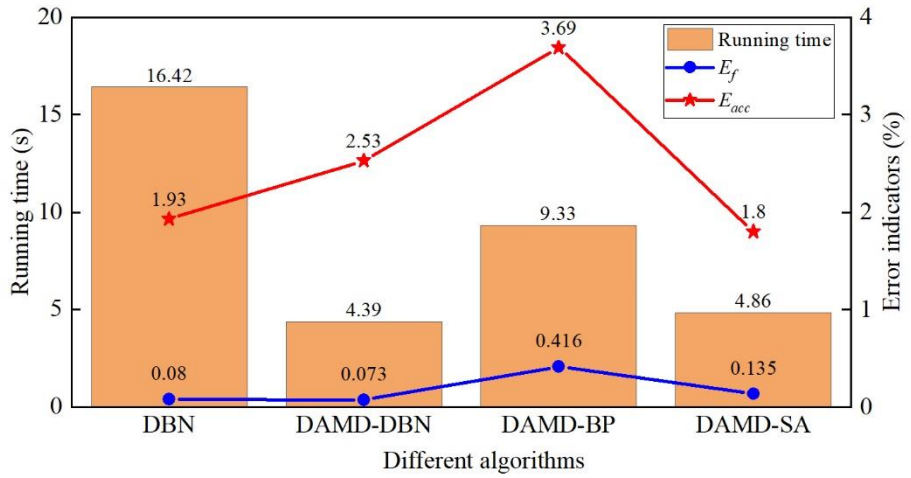


Fig. 18 The comparison of the error indicators and the running time of different algorithms

2015).

As shown in Fig. 18, the error indicators based on the DAMD-BP algorithm are $E_f$=0.416% and $E_{acc}$=3.69%, which is the lowest updating accuracy among the four algorithms. The other three algorithms can update the Bouc-Wen model accurately. However, the proposed method ensures a high updating accuracy, shortens the calculation time, and improves calculation efficiency. It can be seen that the proposed method takes part of instantaneous parameters as input, reduces the input dimension of the DBN, avoids the computational operation. Thus, it improves computational efficiency.

Moreover, DBN overcomes the defects of the BP neural network, such as randomly initializing weight matrix and quickly falling into optimal local values, and has a strong ability of learning generalization. Therefore, the proposed method can describe the relationship between the Bouc-Wen model parameters and the instantaneous parameters more accurately, thus effectively ensuring the accuracy of the modified model. In addition, the proposed method simplifies the steps of nonlinear FEMU without establishing an additional objective function.

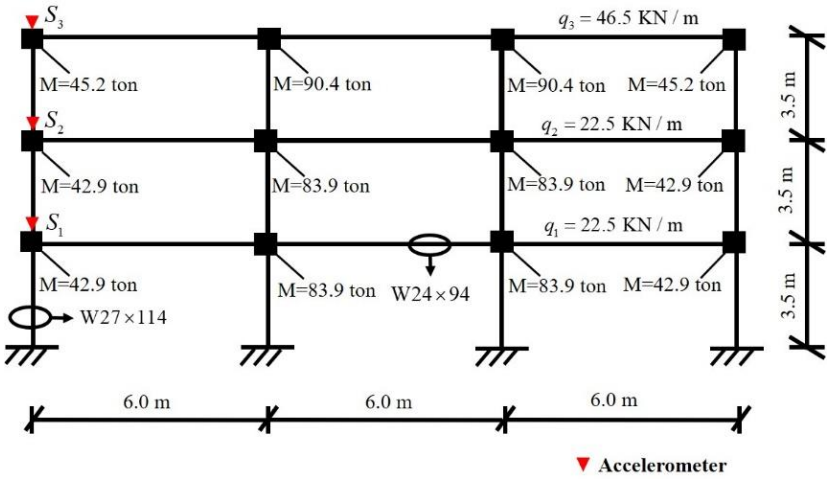


Fig. 19 The three-story Giuffré-Menegotto-Pinto model

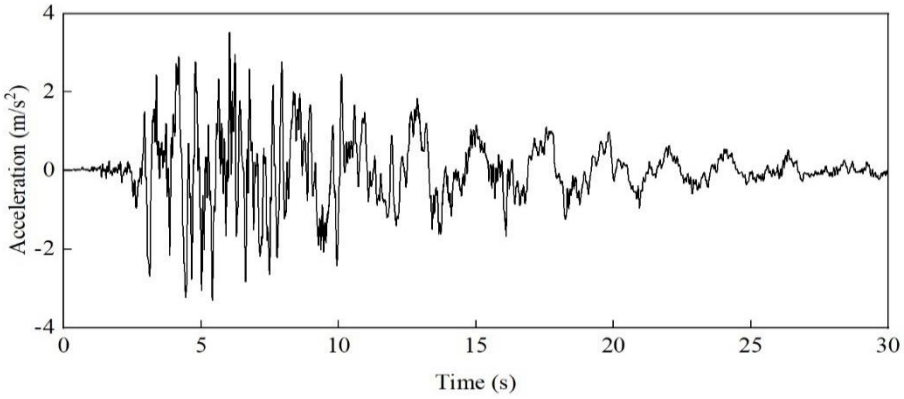


Fig. 20 The acceleration on the 3rd floor of Giuffré-Menegotto-Pinto model

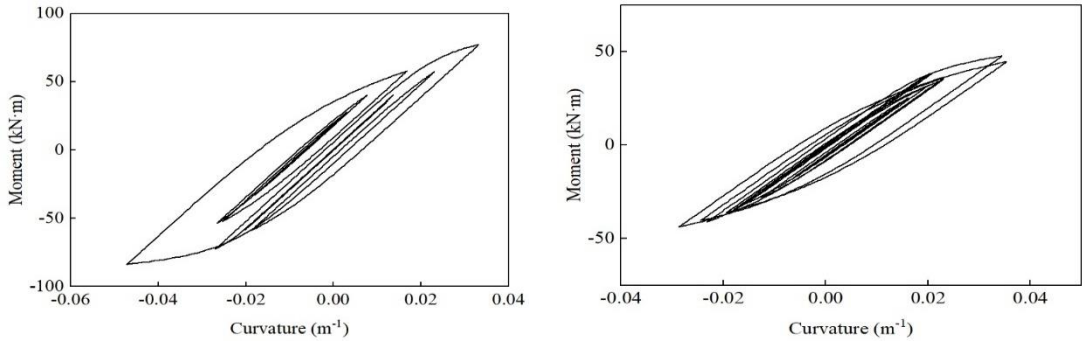


(a) Column elements (b) Beam elements

Fig. 21 The moment-curvature hysteretic curves

### *3.2 Nonlinear model updating for Giuffré-Menegotto-Pinto model*

This section considers a three-layer three-bay steel frame model in OpenSees (McKenna 2011). In this example, all beams and columns of the steel frame model are defined as the nonlinear Beam-Column element with the fiber section. The shape, size, and the distributed load of each layer are shown in Fig. 19. The beam and column sections are adopted the Wide Flange Beams with the sectional dimensions of W24×94 and W27×114, respectively. The Giuffré-Menegotto-Pinto (GMP) model is adopted as the simulated nonlinear hysteresis model. The hysteresis features of the nonlinear model are defined by $F_y$, $E$, and $b$. As a result, six material parameters $F_y^{Beam}$, $E^{Beam}$, $b^{Beam}$, $F_y^{Col}$, $E^{Col}$, $b^{Col}$ are regarded as nonlinear model parameters. Where $F_y^{Beam}$, $E^{Beam}$, $b^{Beam}$ represent the material parameters of the beam elements, and $F_y^{Col}$, $E^{Col}$, $b^{Col}$ denote the material parameters of the column elements.

The initial values of hysteretic material parameters are defined as: $F_y^{Beam}$=12.5 MPa, $E^{Beam}$ =2.0 GPa, $b^{Beam}$=0.16, $F_y^{Col}$=16.5 MPa, $E^{Col}$=2.0 GPa, $b^{Col}$=0.08. The external excitation is the same as section 3.1.1. Moreover, the

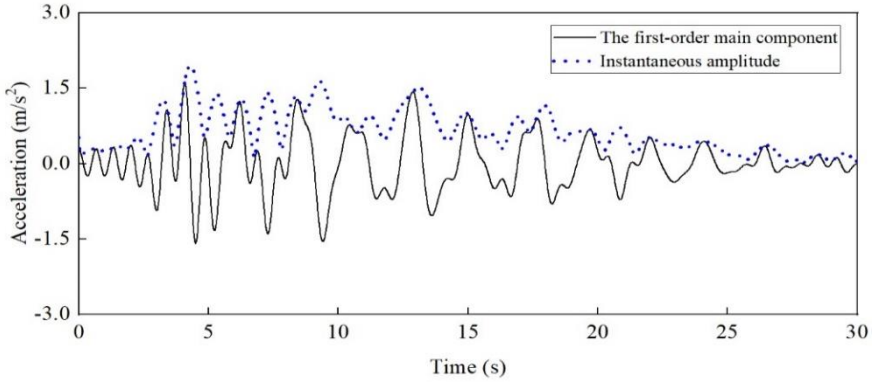


(a) The instantaneous amplitude

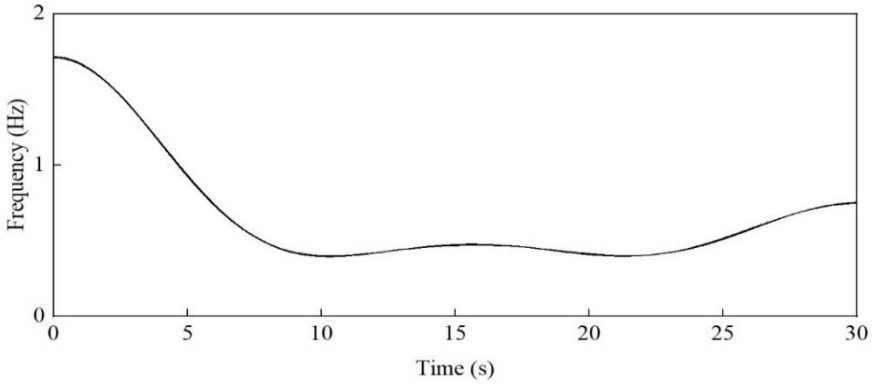


(b) The slow-varying portion of the instantaneous frequency

Fig. 22 The instantaneous characteristics of the main mono-component extracted from the Giuffré-Menegotto-Pinto model under seismic excitation

distributed loads are $q_1$=22.5 KN/m, $q_2$=22.5 KN/m, $q_3$=42.5 KN/m, respectively. The Modified Newton algorithm is employed to calculate the vibration responses, with the sampling frequency of 240 Hz. The 3rd floor simulated acceleration is shown in Fig. 20. The moment-curvature hysteresis curves of beams and columns are demonstrated in Figs. 21 (a)-(b). It can be seen from the hysteretic curves that the structure model shows visible nonlinearity under seismic excitation. The instantaneous parameters of the main mono-component of the 3rd floor acceleration are demonstrated in Fig. 22(a)-(b).

For this example, each hysteresis parameter is uniformly divided into 100 levels within 35% fluctuation of the original. One hundred sets of the six hysteresis parameters are generated by the uniform design matrix $U_{100}(100^6)$. Meanwhile, the corresponding instantaneous parameters are extracted. Then 10% of these instantaneous parameters are selected uniformly. The DBN is trained according to the steps mentioned in section 2.3. At last, the well-trained DBN exports the updated nonlinear model parameters directly.

Table 4 shows the updated hysteretic material parameters. The $E_f$ and $E_{acc}$ are 0.811% and 0.403%, respectively. Fig. 23 compares the 3rd floor acceleration of the calibrated Giuffré-Menegotto-Pinto model and the exact model. Moreover, the extracted $A(t)$ and $f_{sl}(t)$ are shown in Figs. 24(a)-(b). The above results suggest that the nonlinear Giuffré-Menegotto-Pinto model can be updated effectively under seismic excitation.

Table 4 The rectified hysteretic material parameters of the Giuffré-Menegotto-Pinto model without noise

| | $F_y^{Col}$(MPa) | $E^{Col}$(GPa) | $b^{Col}$ | $F_y^{Beam}$(MPa) | $E^{Beam}$(GPa) | $b^{Beam}$ |
|---|---|---|---|---|---|---|
| Updated values | 16.46 | 2.03 | 0.08 | 12.56 | 2.02 | 0.161 |

Gaussian white noise with signal-to-noise ratios of 5%, 10%, 15%, and 20% are added to the simulated acceleration to investigate the influence of noise further. Table 5 lists the rectified hysteretic material parameters and the two error indicators, respectively. These results denote that the proposed method still has relatively high accuracy under the influence of a low noise level.

## 4. Experimental verification

### *4.1 Experimental setup*

A ¼-scale, 3-story steel frame, as shown in Fig. 25, which was rested on the shake table, with one PFD equipped on the 1st floor, is applied for the experimental study. For details of the shake table test, one can refer to (Chen *et al.* 2010). The size of the building structure is 1.22 m×0.61 m ×2.54 m. The total lumped masses of the first, second, and top floor are about 480 kg, 446 kg, and 432 kg, respectively. Before equipping the PFD, several swept-sine tests were carried out to roughly determine the natural

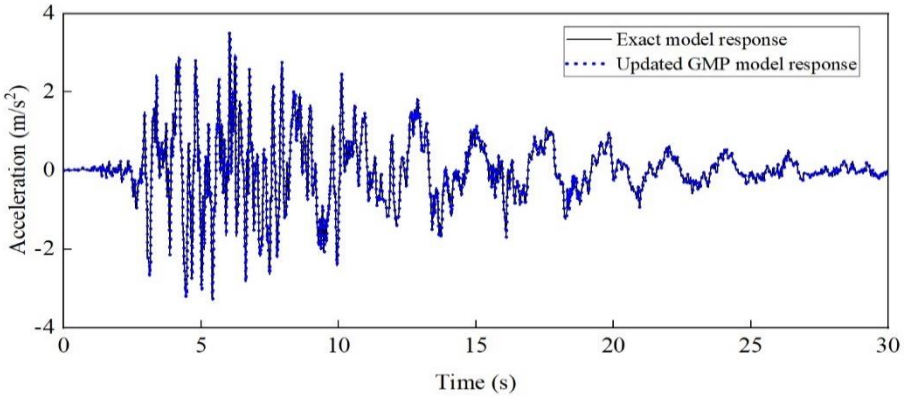


Fig. 23 The acceleration comparison of the updated Giuffré-Menegotto-Pinto model with that of the exact model

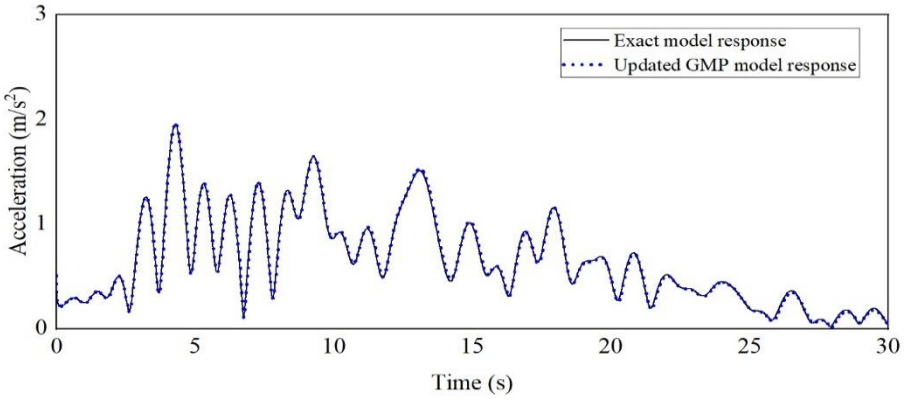


(a) The instantaneous amplitude

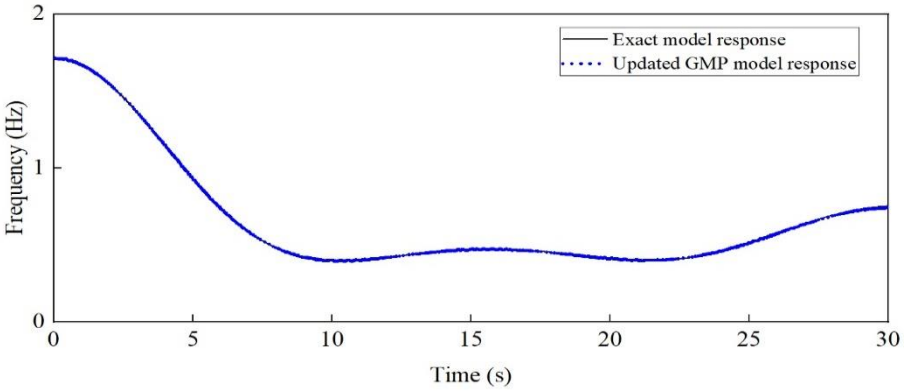


(b) The slow-varying portion of the instantaneous frequency

Fig 24 The comparison of the instantaneous characteristics of the first main mono-component between the updated Giuffré-Menegotto-Pinto model and that of the exact model

Table 5 The updated hysteretic parameters and the two error indicators of the Giuffré-Menegotto-Pinto with various noise levels

| | | $F_y^{Col}$ (MPa) | $E^{Col}$ (GPa) | $b^{Col}$ | $F_y^{Beam}$ (MPa) | $E^{Beam}$ (GPa) | $b^{Beam}$ | $E_f$ (%) | $E_{acc}$ (%) |
|---|---|---|---|---|---|---|---|---|---|
| Exact values | | 16.5 | 2.0 | 0.08 | 12.5 | 2.0 | 0.16 | | |
| Updated values | with 5% noise | 16.48 | 1.99 | 0.08 | 12.19 | 1.98 | 0.172 | 0.31 | 1.55 |
| | with 10% noise | 16.48 | 2.04 | 0.08 | 12.58 | 2.05 | 0.169 | 9.71 | 1.25 |
| | with 15% noise | 16.64 | 1.77 | 0.08 | 11.37 | 2.11 | 0.185 | 9.65 | 8.70 |
| | with 20% noise | 16.51 | 1.96 | 0.08 | 13.21 | 1.95 | 0.188 | 11.3 | 1.46 |


Fig. 25 The ¼ scale, 3-story steel frame

Table 6 The physical parameters of the nonlinear steel frame structure

| $\boldsymbol{M}$ (kg) | $\boldsymbol{C}$ (N·sec/m) | $\boldsymbol{K}$ ($\times 10^6$ N/m) |
|---|---|---|
| $\begin{bmatrix} 480 & 0 & 0 \\ 0 & 446 & 0 \\ 0 & 0 & 432 \end{bmatrix}$ | $\begin{bmatrix} 238.1 & -87.5 & -12.7 \\ -87.5 & 240.0 & -82.9 \\ -12.7 & -82.9 & 159.9 \end{bmatrix}$ | $\begin{bmatrix} 2.865 & -2.344 & 0.440 \\ -2.344 & 3.776 & -1.774 \\ 0.440 & -1.774 & 1.381 \end{bmatrix}$ |

(a) The prototype of PFD


(b) The installation of PFD

Fig. 26 The prototype and installation of PFD

frequencies of the structure as 2.66, 9.46, and 18.70 Hz, respectively. The physical parameters of the structure identified by vibration tests are listed in Table 6.

### *4.2 The nonlinear model parameters of the structure with the PFD*

As shown in Figs. 26 (a)-(b), the PFD used in this study was designed and fabricated in the Structures Engineering Research Laboratory at Missouri University of Science and Technology. The semi-active control algorithm was developed to drive the PFD composed of the Coulomb friction, viscous, and Reid's damper mechanisms (Chen *et al.* 2004). Moreover, the developed control algorithm is used to suppress structural vibration. The semi-active control strategy for a PFD damper can be expressed as

$$f(t)=\begin{cases} \mu N_{pre}\,\mathrm{sgn}[\dot{x}(t)], & when\ e|\dot{x}(t)|+g|\dot{x}(t)|\le N_{pre} \\ \mu g[\xi|x(t)|+|\dot{x}(t)|]\mathrm{sgn}[\dot{x}(t)], & when\ e|\dot{x}(t)|+g|\dot{x}(t)|> N_{pre} \\ -\mu e|x(t)|\le f\le \mu e|x(t)|, & when\ \dot{x}(t)=0 \end{cases} \tag{22}$$

in which $e$ and $g$ denote the two positive gain factors; $x(t)$ and $\dot{x}(t)$ denote the displacement and the velocity of the 1st floor, respectively; $\mu$ is the coefficient of friction of the damper; $N_{pre}$ is the constant normal force applied on the damper; sgn[ ] denotes the Signum function; $\xi$ is the optimization of gain ratio.

Considering the stick phase of the PFD, the friction force on the 1st floor is formulated as

$$f(t)=-c\ddot{x}(t)-kx(t)-\sum_{j=1}^{3} m_j \ddot{z}_g(t) \tag{23}$$

where $\ddot{z}_g(t)$ represents the relative acceleration at the $j$-th building floor concerning the ground acceleration, $c$ and $k$ are the structural damping coefficient and interval stiffness coefficient on the 1st floor.

Table 7 The initial values of the PFD parameters

| | $N_{pre0}$ (N) | $\mu_0$ | $\xi_0$ | $e_0$ (kN-sec/m) | $g_0$ (kN-sec/m) |
|---|---|---|---|---|---|
| Initial values | 89 | 0.35 | 10.64 | 74.533 | 7.005 |

It can be seen in Eqs. (22)-(23) that $N_{pre}$, $\mu$, $\xi$, $e$ and $g$ have a significant influence on the nonlinear vibration responses of the structure. Consequently, the parameters to be updated are selected as $N_{pre}$, $\mu$, $\xi$, $e$, $g$, and the initial values of the PFD parameters defined are shown in Table 7. The steel frame was excited by the compressed 1940 El Centro earthquake with a sampling frequency of 100 Hz. Fig. 27 demonstrates the external seismic excitation.

### *4.3 The nonlinear PFD model updating based on the DBN*

The generated 80 sets of PFD parameters are fed into the nonlinear model to calculate the acceleration response of the 3rd layer. The DAMD and HT methods are used to extract the instantaneous parameters. Then, 10% of the data points are selected with equal time intervals. The 80 groups of PFD parameters and the corresponding instantaneous parameters are used to train the DBN. As the actual PFD parameters are difficult to determine, the test sample is the instantaneous parameters of the measured acceleration in this section. The PFD model is updated following the steps mentioned in section 2.3.

The updated PFD parameters are listed in Table 8. Fig. 28 compares the acceleration of the calibrated nonlinear PFD model and the actual structure. It shows that the acceleration of the calibrated nonlinear model is generally consistent with the measured one. Figs. 29(a)-(b) demonstrate the instantaneous characteristics of the first-order main mono-component.The error indicators $E_f$ and

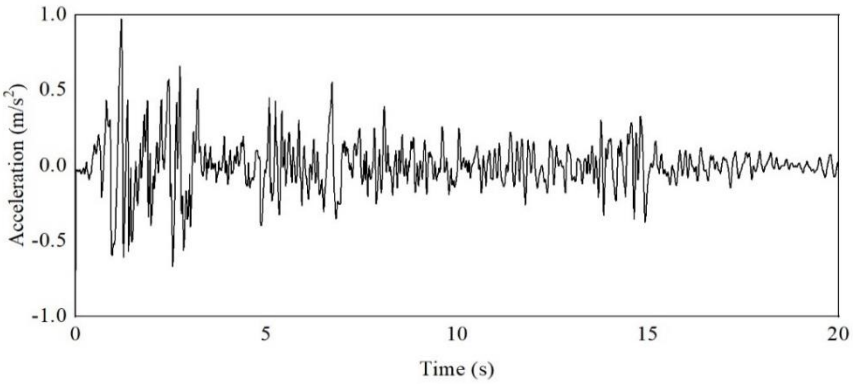


Fig. 27 The acceleration record of the compressed El Centro earthquake

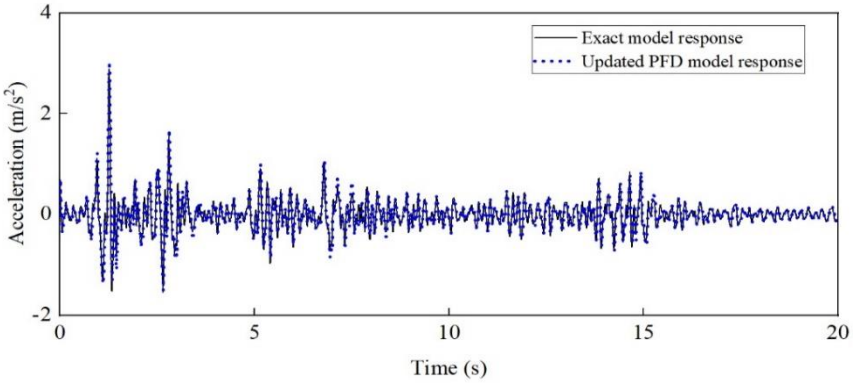


Fig. 28 The acceleration comparison between the updated PFD model and the actual structure under the compressed El Centro earthquake

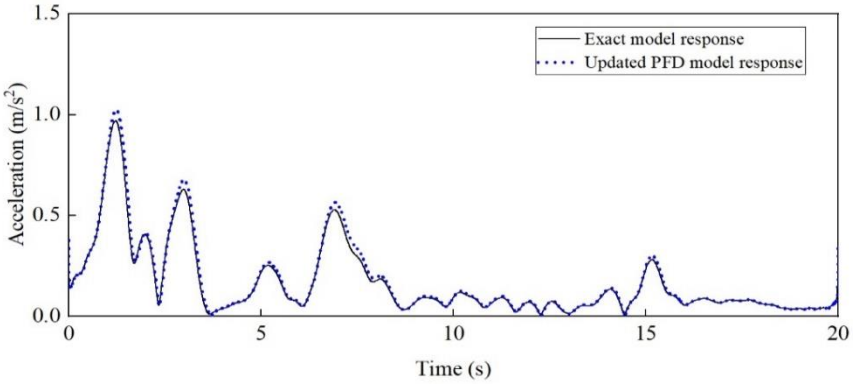


(a) The instantaneous amplitude

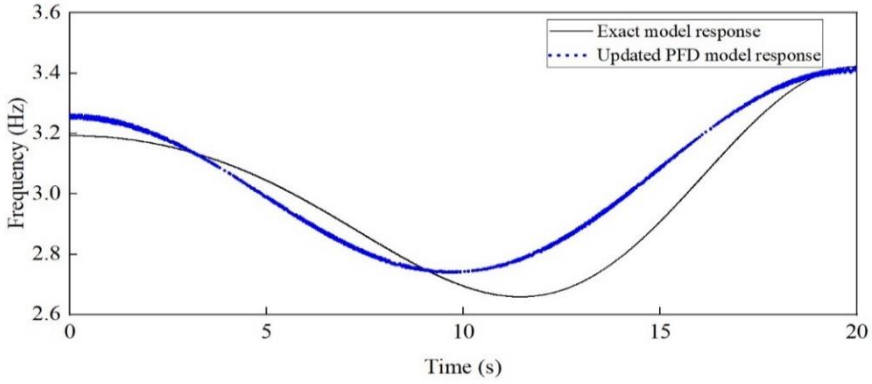


(b) The slow-varying portion of the instantaneous frequency

Fig. 29 The comparison of the instantaneous characteristics of the first main mono-component between the updated PFD model and the actual structure under the compressed El Centro earthquake

Table 8 The updated values of the PFD parameters

| | $N_{pre0}$ (N) | $\mu_0$ | $\xi_0$ | $e_0$ (kN-sec/m) | $g_0$ (kN-sec/m) |
|---|---|---|---|---|---|
| Updated values | 82.0 | 0.35 | 11.61 | 91.87 | 6.770 |

$E_{acc}$ are further calculated as 7.88% and 2.61%, respectively. These results demonstrate that the presented strategy is relatively efficient and accurate.

## 5. Conclusions

This paper developed a DBN-based nonlinear structural model updating methodology. Since the DBN has powerful learning and generalization ability, it can fit the complicated mapping relationship between the instantaneous and nonlinear model parameters. The DBN can be well trained according to the initial training and the retraining process. The updated nonlinear model parameters are obtained by feeding the instantaneous parameters of the measured data into the well-trained DBN. Numerical studies were carried out on the Bouc-Wen model and the Giuffré-Menegotto-Pinto model to verify the effectiveness and accuracy of the presented approach. Besides, experiments have been performed on a three-story steel frame structure. According to the results of simulation and experiment, the following conclusions can be made:

- The presented approach can update the nonlinear model efficiently and accurately, even under different kinds of excitations and various levels of noise effects.
- The DBN is utilized to express the complicated mapping relation between the extracted instantaneous characteristics and the nonlinear model parameters, which dramatically simplifies the process of nonlinear model updating.
- Since the instantaneous parameters used in this paper vary slowly with time, the proposed method can obtain satisfactory results as long as fewer points are selected.
- The proposed method ensures a high updating accuracy, shortens the calculation time, and improves the structural nonlinear model updating efficiency.
- The performance of the proposed method is primarily determined by the training samples and the structure of the DBN. Therefore, it is crucial to select enough representative training samples and optimize the structure of the DBN.

## Acknowledgments

This study was partly supported by the National Natural Science Foundation of China under grand No. 51922036, by the key research and development project of Anhui province under grand No. 1804a0802204, by The Fundamental Research Funds for the Central Universities under grand No. JZ2020HGPB0117, and by the Natural Science Funds for Distinguished Young Scholar of Anhui province under grand No.1708085J06. The results and opinions presented in this paper are those of the authors only and they do not necessarily represent those of the sponsors.

## References

Altunisik, A.C. and Bayraktar, A. (2017), "Manual model updating of highway bridges under operational condition", *Smart Struct. Syst.*, **19**(1), 39-46. https://doi.org/10.12989/sss.2017.19.1.039.

Asadollahi, P., Huang, Y. and Li, J. (2018), "Bayesian finite element model updating and assessment of cable-stayed bridges using wireless sensor data", *Sensor.*, **18**(9), 3057. https://doi.org/10.3390/s18093057.

Asgarieh, E., Moaveni, B. and Stavridis, A. (2014), "Nonlinear finite element model updating of an infilled frame based on identified time-varying modal parameters during an earthquake", *J. Sound Vib.*, **333**(23), 6057-6073. https://doi.org/https://doi.org/10.1016/j.jsv.2014.04.064.

Astroza, R., Nguyen, L.T. and Nestorovic, T. (2016), "Finite element model updating using simulated annealing hybridized with unscented Kalman filter", *Comput. Struct.*, **177**, 176-191. https://doi.org/10.1016/j.compstruc.2016.09.001.

Brownjohn, J.M.W., Moyo, P., Omenzetter, P. and Lu, Y. (2003), "Assessment of highway bridge upgrading by dynamic testing and finite-element model updating", *J. Bridge Eng.*, **8**(3), 162-172. https://doi.org/10.1061/(asce)1084-0702(2003)8:3(162).

Chang, C.C., Chang, T.Y.P. and Xu, Y.G. (2000), "Adaptive neural networks for model updating of structures", *Smart Mater. Struct.*, **9**(1), 59-68. https://doi.org/10.1088/0964-1726/9/1/306.

Chen, C. and Chen, G. (2010), "Shake table tests of a quarter-scale three-storey building model with piezoelectric friction dampers", *Struct. Control Hlth. Monit.*, **11**(4), 239-257. https://doi.org/10.1002/stc.41.

Chen, G. and Chen, C. (2004), "Semiactive control of the 20-story benchmark building with piezoelectric friction dampers", *J. Eng. Mech.*, **130**(4), 393-400. https://doi.org/10.1061/(ASCE)0733-9399(2004)130:4(393).

Chih-Chieh, H. and Chin-Hsiung, L. (2001), "Nonlinear identification of dynamic systems using neural networks", *Comput.-Aid. Civil Infrastr. Eng.*, **16**(1), 28-41. https://doi.org/10.1111/0885-9507.00211.

El-Borgi, S., Choura, S., Ventura, C., Baccouch, M. and Cherif, F. (2005), "Modal identification and model updating of a reinforced concrete bridge", *Smart Struct. Syst.*, **1**(1), 83-101. https://doi.org/10.12989/sss.2005.1.1.083.

Feldman, M. (1997), "Non-linear free vibration identification via the Hilbert transform", *J. Sound Vib.*, **208**(3), 475-489. https://doi.org/10.1006/jsvi.1997.1182.

Fischer, A. and Igel, C. (2014), "Training restricted Boltzmann machines: An introduction", *Pattern Recog.*, **47**(1), 25-39. https://doi.org/10.1016/j.patcog.2013.05.025.

Hasancebi, O. and Dumlupinar, T. (2013), "Linear and nonlinear model updating of reinforced concrete T-beam bridges using artificial neural networks", *Comput. Struct.*, **119**, 1-11. https://doi.org/10.1016/j.compstruc.2012.12.017.

Hemez, F.M. and Doebling, S.W. (2001), "Review and assessment of model updating for non-linear transient dynamics", *Mech. Syst. Signal Pr.*, **15**, 45. https://doi.org/10.1006/mssp.2000.1351.

Hinton, G.E. (2012), *Neural Networks: Tricks of the Trade: Second Edition*, Springer Berlin Heidelberg, Heidelberg, Berlin.

Hinton, G.E. and Salakhutdinov, R.R. (2006), "Reducing the dimensionality of data with neural networks", *Sci.*, **313**(5786), 504-507. https://doi.org/10.1126/science.1127647.

Hoa, T.N., Khatir, S., De Roeck, G., Long, N.N., Thanh, B.T. and Wahab, M.A. (2020), "An efficient approach for model updating of a large-scale cable-stayed bridge using ambient vibration measurements combined with a hybrid metaheuristic search algorithm", *Smart Struct. Syst.*, **25**(4), 487-499.

https://doi.org/10.12989/sss.2020.25.4.487.
Hofmeister, B., Bruns, M. and Rolfes, R. (2019), "Finite element model updating using deterministic optimisation: A global pattern search approach", *Eng. Struct.*, **195**, 373-381. https://doi.org/10.1016/j.engstruct.2019.05.047.
Huang, Y., Zhang, H., Li, H. and Wu, S. (2021), "Recovering compressed images for automatic crack segmentation using generative models", *Mech. Syst. Signal Pr.*, **146**, 107061. https://doi.org/https://doi.org/10.1016/j.ymssp.2020.107061.
Le Roux, N. and Bengio, Y. (2010), "Deep belief networks are compact universal approximators", *Neur. Comput.*, **22**(8), 2192-2207. https://doi.org/10.1162/neco.2010.08-09-1081.
Lei, Y., Wang, H.F. and Shen, W.A. (2012), "Update the finite element model of Canton Tower based on direct matrix updating with incomplete modal data", *Smart Struct. Syst.*, **10**(4-5), 471-483. https://doi.org/10.12989/sss.2012.10.4_5.471.
Li, S., Zhao, X. and Zhou, G. (2019), "Automatic pixel-level multiple damage detection of concrete structure using fully convolutional network", *Comput.-Aid. Civil Infrastr. Eng.*, **34**(7), 616-634. https://doi.org/https://doi.org/10.1111/mice.12433.
Lu, Y. and Tu, Z.G. (2004), "A two-level neural network approach for dynamic FE model updating including damping", *J. Sound Vib.*, **275**(3-5), 931-952. https://doi.org/10.1016/s0022-460x(03)00796-x.
Mckenna, F. (2011), "OpenSees: A framework for earthquake engineering simulation", *Comput. Sci. Eng.*, **13**(4), 58-66. https://doi.org/10.1109/mcse.2011.66.
Mohamed, A.R., Dahl, G.E. and Hinton, G. (2012), "Acoustic modeling using deep belief networks", *IEEE Trans. Audio Speech Language Pr.*, **20**(1), 14-22. https://doi.org/10.1109/tasl.2011.2109382.
Mordini, A., Savov, K. and Wenzel, H. (2007), "The finite element model updating: a powerful tool for structural health monitoring", *Struct. Eng. Int.*, **17**(4), 352-358. https://doi.org/10.2749/101686607782359010.
Naranjo-Pérez, J., Jiménez-Alonso, J.F., Pavic, A. and Sáez, A. (2020), "Finite-element-model updating of civil engineering structures using a hybrid UKF-HS algorithm", *Struct. Infrastr. Eng.,* 1-18. https://doi.org/10.1080/15732479.2020.1760317.
Naseralavi, S.S., Shojaee, S. and Ahmadi, M. (2016), "Modified gradient methods hybridized with Tikhonov regularization for damage identification of spatial structure", *Smart Struct. Syst.*, **18**(5), 839-864. https://doi.org/10.12989/sss.2016.18.5.839.
Ni, P.H. and Ye, X.W. (2019), "Nonlinear finite element model updating with a decentralized approach", *Smart Struct. Syst.*, **24**(6), 683-692. https://doi.org/10.12989/sss.2019.24.6.683.
Park, Y.S., Kim, S., Kim, N. and Lee, J.J. (2017), "Finite element model updating considering boundary conditions using neural networks", *Eng. Struct.*, **150**, 511-519. https://doi.org/10.1016/j.engstruct.2017.07.032.
Pirmoradi, S., Teshnehlab, M., Zarghami, N. and Sharifi, A. (2020), "The self-organizing restricted boltzmann machine for deep representation with the application on classification problems", *Exp. Syst. Appl.*, **149**, 113286. https://doi.org/10.1016/j.eswa.2020.113286.
Qiao, J., Wang, G., Li, X. and Li, W. (2018), "A self-organizing deep belief network for nonlinear system modeling", *Appl. Soft Comput.*, **65**, 170-183. https://doi.org/https://doi.org/10.1016/j.asoc.2018.01.019.
Wang, Z.C., Xin, Y. and Ren, W.X. (2015), "Nonlinear structural model updating based on instantaneous frequencies and amplitudes of the decomposed dynamic responses", *Eng. Struct.*, **100**, 189-200. https://doi.org/10.1016/j.engstruct.2015.06.002.
Wang, Z.C., Xin, Y., Xing, J.F. and Ren, W.X. (2017), "Hilbert low-pass filter of non-stationary time sequence using analytical mode decomposition", *J. Vib. Control*, **23**(15), 2444-2469. https://doi.org/10.1177/1077546315617408.
Weng, S., Xia, Y., Xu, Y.L. and Zhu, H.P. (2011), "Substructure based approach to finite element model updating", *Comput. Struct.*, **89**(9-10), 772-782. https://doi.org/10.1016/j.compstruc.2011.02.004.
Xu, W., Peng, H., Zeng, X., Zhou, F., Tian, X. and Peng, X. (2019), "Deep belief network-based AR model for nonlinear time series forecasting", *Appl. Soft Comput.*, **77**, 605-621. https://doi.org/https://doi.org/10.1016/j.asoc.2019.02.006.
Yuen, K.V. and Kuok, S.C. (2011), "Bayesian methods for updating dynamic models", *Appl. Mech. Rev.*, **64**(1), 1-18. https://doi.org/10.1115/1.4004479.
Yun, C.B. and Bahng, E.Y. (2000), "Substructural identification using neural networks", *Comput. Struct.*, **77**(1), 41-52. https://doi.org/10.1016/s0045-7949(99)00199-6.
Zapico, J.L., Gonzalez-Buelga, A., Gonzalez, M.P. and Alonso, R. (2008), "Finite element model updating of a small steel frame using neural networks", *Smart Mater. Struct.*, **17**(4), 045016. https://doi.org/10.1088/0964-1726/17/4/045016.
Zhang, J., Wan, C.F. and Sato, T. (2013), "Advanced Markov Chain Monte Carlo approach for finite element calibration under uncertainty", *Comput.-Aid. Civil Infrastr. Eng.*, **28**(7), 522-530. https://doi.org/10.1111/j.1467-8667.2012.00802.x.
Zhou, Y., Pei, Y., Li, Z., Fang, L., Zhao, Y. and Yi, W. (2020), "Vehicle weight identification system for spatiotemporal load distribution on bridges based on non-contact machine vision technology and deep learning algorithms", *Measure.*, **159**, 107801. https://doi.org/https://doi.org/10.1016/j.measurement.2020.107801.

*CC*